

---

## An Adaptive Finite Element Strategy for Analysis of Air Lubrication in the Head-Disk Interface of a Hard Disk Drive

Praveen Holani\* — Sinan Müftü\*\*

John F. Welch Technology Center  
GE India Technology Center Pvt. Ltd.  
Export Promotion Industrial Park, Bangalore - 560 066, India

\*\* Department of Mechanical and Industrial Engineering  
Northeastern University  
Boston, MA 02115, USA  
s.muftu@neu.edu

---

*RÉSUMÉ.* En cet article une solution finie d'élément de l'équation modifiée de Reynolds en utilisant les éléments quadrilatéraux isoparamétriques et bilinéaires avec une stratégie engrenante adaptative est présentée. La méthode hydrodynamique modifiée de rigidité (Smith, 1995) a été employée pour obtenir une solution couplée de l'équation de galet pneumatique avec les équations d'équilibre de glisseur. L'algorithme engrenant adaptatif basé par étiquette de sommet de Cheng et autres (1999) a été également mis en application. Le problème est au commencement résolu avec une maille régulière de Fe de quadrilatère. L'adaptation de maille (h-amélioration) est basée sur les gradients relatifs de pression dans la solution initiale, et sur la géométrie du glisseur. L'amélioration est mise en application sur un élément existant, si préréglés les critères sur le gradient de pression et/ou la géométrie de glisseur sont excédés. La méthode est décrite en détail. Des exemples sont présentés.

*ABSTRACT.* In this paper a finite element solution of the modified Reynolds equation using isoparametric, bilinear quadrilateral elements with an adaptive meshing strategy is presented. The modified hydrodynamic stiffness method (Smith, 1995) was used to obtain a coupled solution of the air bearing equation with the slider equilibrium equations. The vertex label based adaptive meshing algorithm of Cheng et al. (1999) was also implemented. The problem is initially solved with a regular quadrilateral FE mesh. The mesh adaptation (h-refinement) is based on the relative pressure gradients in the initial solution, and on the geometry of the slider. The refinement is implemented on an existing element, if preset criteria on the pressure gradient and/or slider geometry are exceeded. The method is described in detail. Examples are presented. Two types of sliders have been used, namely the 50% taper flat slider, and the negative air bearing slider.

*MOTS-CLÉS :* aérez la lubrification, éléments finis, maille adaptative, interface de tête-disque

*KEYWORDS :* air lubrication, finite elements, adaptive mesh, head-disk interface

---

## 1. Introduction

Today, magnetic hard disk drives (HDD's) constitute a large portion of digital data storage capacity. The overall performance of hard disk drives may appear to depend on simple components; however their design and manufacture require leading-edge capabilities in device modeling, materials science, photolithography, vacuum deposition processes, ion beam etching, reliability testing, mechanical design, machining, air bearing design, tribology, and head/disk interface (Mee *et al.*, 1996, Bhushan, 1996).

Magnetic recording requires relative motion between the magnetic media and a read-write head (Mee *et al.*, 1996). In a computer HDD a shaped slider, attached to a flexible suspension-arm, glides over a rigid cylindrical disk, which rotates at rotational rates reaching 10,000 rpm or more. The trailing edge of the slider contains a built-in magnetic read-write head (Fig. 1). Different tracks over the magnetic disk are addressed by moving the suspension-arm in the radial direction. A small gap ( $h_{min}$ ) on the order of 5 – 20 nm is maintained between the disk and the slider. The size of the gap is dictated by the signal-to-noise ratio of the magnetic recording, which deteriorates exponentially with increasing separation between the magnetic medium and the read-write head (Mee *et al.*, 1996). Air lubrication between the rotating disk and the slider is critical to maintain this gap; a delicate balance is established between the suspension preload, air bearing pressure and restoring forces due to small perturbations from the equilibrium flying height.

The numerical modeling of the pivoted slider bearing provides a means to evaluate different configurations without actually having to build them. This involves the simultaneous solution of the two dimensional (2D) compressible Reynolds Equation (RE) with slip flow correction for the air bearing and the force and moment equilibrium equations for the slider. The 2D compressible RE is a non-linear partial differential equation. Since the analytical solution of the Reynolds equation is not possible for a generic slider, a numerical solution is used.

Different spatial discretization methods have been used for solving the non-linear, compressible RE for the head-disk interface (HDI) problem. These include finite difference (FD) (White *et al.*, 1980, Castelli *et al.*, 1968), finite volume (FV)

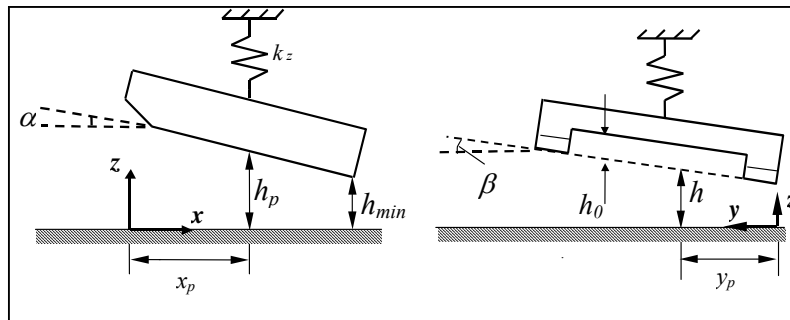


**Figure 1.** Schematic description of the pivoted slider bearing at equilibrium.

(Wu *et al.*, 2000, Wu *et al.*, 1999) and finite element (FE) methods (Smith *et al.*, 1995, Wahl, 1994, Garcia-Suarez, 1984, Hendricks, 1988, Kubo *et al.*, 1988, Peng *et al.*, 1995). The slider equilibrium position is coupled to the air pressure, also in a non-linear manner. The coupling between the two sets of equations can be handled by considering the dynamical effects of the system. In that case the squeeze film effect for the RE and the translational and rotational inertia effects for the slider need to be considered (Tang, 1972, Ono, 1972, White *et al.*, 1980, Miu *et al.*). The steady state flying height can be found by the transient solution approach by running the code until steady state conditions are found. Alternatively, the coupled solution can be obtained by formulating the problem entirely for steady state (Yamaura *et al.*, 1990, Choi *et al.*, 1994, Smith *et al.*, 1995, Wahl, 1994).

One of the challenging problems with numerical methods is the need to represent a continuous domain with a spatially discretized mesh. The FD method typically requires a structured mesh and is limited in the choice of mesh refinement that it offers. Wu and Bogoy presented a FV method with unstructured triangular meshing to solve the modified RE. They implemented a three level adaptive meshing strategy based on Delaunay triangulation (Wu *et al.*, 1999, Wu *et al.*, 2000). In general, use of a structured mesh is not required in the FE method. This trait is very suitable for local adaptive refinement in regions where the solution displays large gradients of the solution parameter or the slider geometry changes abruptly. In this paper a finite element solution of the modified RE using isoparametric, bilinear quadrilateral elements with an adaptive meshing strategy is presented.

In this paper the *modified hydrodynamic stiffness* method (Smith *et al.*, 1995, Wahl, 1994) was used to obtain a coupled solution of the air bearing equation with the slider equilibrium equations. The adaptive meshing algorithm given by Cheng *et al.* was also implemented (Cheng *et al.*, 1989). A computationally efficient storage for the global stiffness matrix and solution methods for the solution involving large number of degrees of freedom were investigated and used (Holani, 2002).

Here, the problem is initially solved with a regular quadrilateral FE mesh. The mesh adaptation (*h*-refinement) is based on a) the relative pressure gradients in the initial solution, and b) the geometry of the slider. The refinement is implemented on an existing element, if preset criteria on the pressure gradient and/or slider geometry are exceeded. Such an element is simply divided into smaller ones keeping the original element boundaries intact. This approach could result in dangling nodes, where an element with mid-side nodes is joined to a linear element with no such nodes. In this work, the admissible function algorithm, of Cheng *et al.* (Cheng *et al.*, 1989), is implemented to prevent such dangling nodes. This algorithm describes a way to subdivide a few adjacent elements apart from the master element, which causes the dangling nodes. A bandwidth reduction algorithm has been applied in order to keep the bandwidth of the system as small as possible for efficient memory management and minimizing computational time (Collins, 1973).

## 2. Governing Equations and Boundary Conditions

### 2.1. Reynolds Equation

The airflow in the head-disk interface (HDI) of a HDD is modeled by using the modified Reynolds equation. As the spacing in the HDI is smaller than the molecular mean free path ( $\lambda$ ) of air, the continuum theory does not apply, and rarefaction effects must be considered. To this end the first order slip-flow correction was introduced by Burgdorfer (Burgdofer, 1959), and the second order slip flow correction by Hsia and Domoto (Hsia *et al.*, 1983). Fukui and Kaneko rederived the Reynolds equation based on the Boltzman equation (Fukui *et al.*, 1988). In standard vector notation, the general form of the two dimensional compressible Reynolds equation with slip flow corrections is given as follows:

$$\nabla \cdot \{ ph^3 Q_r \nabla p \} = 6\mu (\vec{V} \cdot \nabla (ph)) + 12\mu \frac{\partial}{\partial t} (ph), \quad (1)$$

where  $\nabla$  is the gradient operator,  $p$  is the air pressure,  $h$  is the head-to-disk interfacial clearance,  $\vec{V} = V_x \hat{i} + V_y \hat{j}$  is the disk velocity with the components  $V_x$  and  $V_y$  in the  $x$ - and  $y$ -directions, respectively,  $\mu$  is the dynamic viscosity of air,  $t$  is time, and  $Q_r$  is the flow rate correction coefficient due to slip-flow. This coefficient depends on the Knudsen number  $Kn = \lambda/h$ , and, for different slip-flow models it is defined as follows:

$$\begin{array}{ll} Q_r = 1, & \text{classical compressible RE,} \\ Q_r = 1 + 6Kn, & \text{for 1<sup>st</sup> order slip-flow correction,} \\ Q_r = 1 + 6Kn + 6Kn^2, & \text{for 2<sup>nd</sup> order slip-flow correction,} \\ Q_r = f(Kn), & \text{for Boltzman Reynolds equation.} \end{array}$$

The functional dependence of the flow correction for the Boltzman RE is derived by Fukui and Kaneko (Fukui *et al.*, 1988, Fukui *et al.*, 1990) and also presented by Crone *et al.* (Crone *et al.*, 1992). In this work the second order slip flow correction is considered, however the method developed is valid for all of the cases. Using the relation  $p\lambda = p_a \lambda_a$  for constant temperature (Burgdofer, 1959) the steady state form of the second-order modified, compressible RE becomes:

$$\nabla \cdot \left\{ \left[ ph^3 + 6p_a \lambda_a h^2 + 6(p_a \lambda_a)^2 \frac{h}{p} \right] \nabla p \right\} = 6\mu (\vec{V} \cdot \nabla (ph)) \quad (2)$$

where  $\lambda_a$  is the molecular mean free path, and  $p_a$  is the pressure of air at standard ambient conditions. The air pressure is assumed to be ambient  $p = p_a$  on the outside periphery of the slider.

## 2.2. Slider Equilibrium Equations

The HDD slider is attached to a suspension arm which provides three degrees of freedom (dof) as shown in Fig. 1;  $h_p$  is the translational degree of freedom (dof), in the direction perpendicular to the disk surface; and  $\alpha$  and  $\beta$  are the pitch and the roll degrees of rotational freedom, about the  $y$ - and  $x$ -axes, respectively. The translation in the vertical direction is associated with the vertical stiffness  $k_z$  of the suspension, whereas the pitch angle and the roll angles are related to the rotational stiffnesses,  $k_\alpha$  and  $k_\beta$ , respectively. The steady state force and moment balance about the “equilibrium” state of the slider yields:

$$\begin{bmatrix} k_z & 0 & 0 \\ 0 & k_\alpha & 0 \\ 0 & 0 & k_\beta \end{bmatrix} \begin{Bmatrix} dh_p \\ d\alpha \\ d\beta \end{Bmatrix} = \begin{Bmatrix} \int_A p dA \\ \int_A p(x_p - x) dA \\ \int_A p(y_p - y) dA \end{Bmatrix} - \begin{Bmatrix} F^{ext} \\ M_\alpha^{ext} \\ M_\beta^{ext} \end{Bmatrix} \quad (3)$$

where  $dh_p$ ,  $d\alpha$  and  $d\beta$  are the small perturbations in the translational and rotational degrees of freedom of the slider about the equilibrium state,  $a$  is the area of the footprint of the slider,  $f^{ext}$  is the external normal load including the preload in the slider spring and  $M_\alpha^{ext}$  and  $M_\beta^{ext}$  are the external moments acting on the system. for notational simplicity eqn (3) is expressed by using the following matrix notation:

$$\mathbf{K}_s \mathbf{du} = \mathbf{f}(p) - \mathbf{f}^{ext} \quad (4)$$

where the slider dof vector is  $\mathbf{u} = \{h_p \ \alpha \ \beta\}^T$  and the slider stiffness matrix is  $\mathbf{K}_s$ , external force vector is  $\mathbf{f}^{ext}$  and the air bearing load vector is  $\mathbf{f}$ . Note that the  $\mathbf{f}$  vector is a function of air pressure  $p$  which in turn is a function of slider position  $\mathbf{u}$ . Thus, Eqn (4) is a non-linear equation. The geometric shape of the slider is given as:

$$h(x, y) = h_p + \alpha(x_p - x) + \beta(y - y_p) + h_0(x, y) \quad (5)$$

where  $h_0(x, y)$  is the slider contour with respect to the reference surface, as shown in Fig 1.

## 2.3. Simultaneous Solution of Slider and Reynolds Equations

The Reynolds equation and the slider equilibrium equations are coupled. In this work the slider equilibrium is obtained by using the *modified hydrodynamic stiffness* method (Wahl, 1994) described in Section 2.3.1. The air pressure is obtained by solving non-linear RE numerically as described in Section 2.3.2. The slider equilibrium and the air pressure are solved iteratively as described in Section 3.6.

### 2.3.1. Solution of the Slider Equilibrium Equations

In the *modified hydrodynamic stiffness* method (Wahl, 1994), Eqns (2) and (4) are solved in an iterative manner. First, Eqn. (4) is linearized by using multivariable Taylor series expansion on the air bearing load  $\mathbf{f}(p(\mathbf{u}))$ , which yields (Holani, 2002):

$$(\mathbf{K}_s - \mathbf{K}_t^{(n)})\mathbf{du} = \mathbf{f}(p)^{(n)} - \mathbf{f}^{\text{ext}} \quad (6)$$

where  $\mathbf{K}_t^{(n)}$  is the tangent (air-bearing) stiffness matrix and  $\mathbf{f}(p)^{(n)}$  is the external load vector at iteration level  $n$ . In general, the tangent stiffness matrix is defined as  $\mathbf{K}_t^{(n)} = \partial \mathbf{f}^{(n)} / \partial \mathbf{u}$ . In the *modified hydrodynamic stiffness* approach, however, the tangent stiffness matrix is obtained by considering the geometric relation for the slider shape given by Eqn (5) and by using the chain rule of differentiation (Wahl, 1994). Then the tangent stiffness matrix becomes:

$$\mathbf{K}_t^{(n)} = \left( \frac{\partial \mathbf{f}}{\partial h} \frac{\partial h}{\partial \mathbf{u}} \right)^{(n)} = \begin{bmatrix} \int_A \left( \frac{\partial p}{\partial h} \right)^{(n)} dA & \int_A \left( \frac{\partial p}{\partial h} \right)^{(n)} (x_p - x) dA & - \int_A (y_p - y) \left( \frac{\partial p}{\partial h} \right)^{(n)} dA \\ \int_A \left( \frac{\partial p}{\partial h} \right)^{(n)} (x_p - x) dA & \int_A \left( \frac{\partial p}{\partial h} \right)^{(n)} (x_p - x)^2 dA & - \int_A \left( \frac{\partial p}{\partial h} \right)^{(n)} (x_p - x)(y_p - y) dA \\ \int_A \left( \frac{\partial p}{\partial h} \right)^{(n)} (y_p - y) dA & \int_A \left( \frac{\partial p}{\partial h} \right)^{(n)} (x_p - x)(y_p - y) dA & \int_A \left( \frac{\partial p}{\partial h} \right)^{(n)} (y_p - y)^2 dA \end{bmatrix} \quad (6)$$

Note that all terms of  $\mathbf{K}_t^{(n)}$  depend on the pressure gradient  $(\partial p / \partial h)^{(n)}$ . An expression for this variable is obtained by considering a linear perturbation of the modified RE by:

$$h = h^{(n)} - \varepsilon \quad \text{and} \quad p = p^{(n)} + \varepsilon \psi \quad (7)$$

where  $\psi = \frac{\partial p^{(n)}}{\partial h}$  and  $\varepsilon$  is a small perturbation parameter. Neglecting the higher order terms of  $\varepsilon$ , when combining Eqns. (2) and (7) yields:

$$\begin{aligned} & \frac{\partial}{\partial x} \left\{ C_1 \psi \frac{\partial p^{(n)}}{\partial x} + C_2 \frac{\partial \psi}{\partial x} - C_3 \frac{\partial p^{(n)}}{\partial x} \right\} + \frac{\partial}{\partial y} \left\{ C_1 \psi \frac{\partial p^{(n)}}{\partial y} + C_2 \frac{\partial \psi}{\partial y} - C_3 \frac{\partial p^{(n)}}{\partial y} \right\} \\ & = 6\mu V_x \left\{ h^{(n)} \frac{\partial \psi}{\partial x} + \psi \frac{\partial h^{(n)}}{\partial x} - \frac{\partial p^{(n)}}{\partial x} \right\} + 6\mu V_y \left\{ h^{(n)} \frac{\partial \psi}{\partial y} + \psi \frac{\partial h^{(n)}}{\partial y} - \frac{\partial p^{(n)}}{\partial y} \right\} \end{aligned} \quad (8)$$

where

$$\begin{aligned}
C_1 &= \left(h^{(n)}\right)^3 + 6\lambda_a p_a \frac{\left(h^{(n)}\right)^2}{p^{(n)}} - 6\left(\lambda_a p_a\right)^2 \frac{h^{(n)}}{\left(p^{(n)}\right)^2} \\
C_2 &= p^{(n)} \left(h^{(n)}\right)^3 + 6\lambda_a p_a \left(h^{(n)}\right)^2 + 6\left(\lambda_a p_a\right)^2 \frac{h^{(n)}}{p^{(n)}} \\
C_3 &= 3p^{(n)} \left(h^{(n)}\right)^2 + \frac{6\left(\lambda_a p_a\right)^2}{p^{(n)}} + 12\lambda_a p_a h^{(n)}
\end{aligned} \tag{9}$$

with the boundary condition  $\psi = 0$  on the boundary. A finite element formulation of Eqn (8) is obtained by using the Galerkin finite element method (Zienkiewicz *et al.*, 2000). In this work quadratic elements with bilinear shape functions are used in an isoparametric formulation. The finite element form of Eqn. (8) is expressed in matrix notation as follows:

$$\mathbf{k}_{\psi}^{(e)} \boldsymbol{\Psi}^{(e)} = \mathbf{r}_{\psi}^{(e)} \tag{10}$$

where  $\mathbf{k}_{\psi}^{(e)}$  is the element stiffness matrix for pressure gradient calculations,  $\boldsymbol{\Psi}^{(e)} = \{\psi_1 \ \psi_2 \ \psi_3 \ \psi_4\}^T$  is the vector for pressure gradients at element nodes and  $\mathbf{r}_{\psi}^{(e)}$  is the right hand side vector. The details of the element stiffness matrix and the right hand side vector are given in Appendix 1. Note that the superscript indicating the iteration level ( $n$ ) is omitted from Eqn (10) for notational simplicity. The element stiffness matrix and the right hand side vector of each element are assembled into a global system of equations. This yields the following matrix equation:

$$\mathbf{K}_{\psi}^{(n)} \boldsymbol{\Psi}^{(n)} = \mathbf{R}_{\psi}^{(n)} \tag{11}$$

where  $\mathbf{K}_{\psi}^{(n)}$  is the global stiffness matrix for pressure gradient calculations,  $\boldsymbol{\Psi}_{n_d \times 1}^{(n)}$  is the global degrees of freedom for pressure gradients,  $\mathbf{R}_{\psi}^{(n)}$  is the global right hand side vector and  $n_d$  is the total number of dofs. Solving Eqn (11) yields the pressure gradient  $\psi^{(n)} = (\partial p / \partial h)^{(n)}$  at each node. Substituting  $\boldsymbol{\Psi}^{(n)}$  into Eqn (6) yields the simplified air-bearing coupling matrix. The solution algorithm is described in Section 3.6.

### 2.3.2. Solution the Modified Reynolds Equation

In addition to finding the pressure gradients, the coupling algorithm also requires calculation of the pressure value  $p$  at each node. As the modified RE (2) is non-linear, the solution is obtained iteratively:

$$p_i^{(m+1)} = p_i^{(m)} + dp_i^{(m)} \text{ for } i = 1, \dots, n_d \quad (12)$$

where  $m$  is the iteration level for the pressure calculations. The pressure correction vector for the entire solution domain  $\mathbf{dP}_{n_d \times 1}^{(m)} = \{dp_1^{(m)} \ dp_2^{(m)} \ \dots \ dp_{n_d}^{(m)}\}^T$  is obtained by finite element method. Eqn (2) is linearized substituting (12) into (2) and neglecting terms that are non-linear in  $dp_i^{(m)}$ . The Galerkin method is used to obtain the weak form of the linearized equation. The finite element method is implemented by using isoparametric, bilinear quadrilateral elements. The element stiffness equations are symbolically represented as follows:

$$\mathbf{k}_p^{(e)} \mathbf{dp}^{(e)} = \mathbf{r}_p^{(e)} \quad (13)$$

where  $\mathbf{k}_{p_{4 \times 4}}^{(e)}$  is the element stiffness matrix for pressure calculations,  $\mathbf{dp}^{(e)} = \{dp_1 \ dp_2 \ dp_3 \ dp_4\}^T$  is the nodal degree of freedom vector for incremental change in pressure and  $\mathbf{r}_{p_{4 \times 1}}^{(e)}$  is the right hand side vector. The details of  $\mathbf{k}_p^{(e)}$  and  $\mathbf{r}_p^{(e)}$  are given in Appendix 2. Assembly of the element stiffness matrices and application of ambient pressure boundary conditions around the outer periphery of the slider results in the global stiffness equations:

$$\mathbf{K}_p^{(m)} \mathbf{dP}^{(m)} = \mathbf{R}_p^{(m)} \quad (14)$$

where  $\mathbf{K}_{p_{n_d \times n_d}}^{(m)}$  is the global tangent stiffness matrix for air pressure and  $\mathbf{R}_{p_{n_d \times 1}}^{(m)}$  is the global right hand side vector. Solving Eqn (14) yields the change in pressure  $dp$  at each node. The pressure for each node is obtained iteratively as described in Section 3.6.

### 3. Adaptive Subdivision of the Finite Element Mesh

The accuracy of the finite element solution depends on the mesh density. In particular, for the solution of the Reynolds equation, a high mesh density is required in regions of large pressure gradients. The cost of analysis becomes prohibitively expensive if the number of elements in the mesh is too large. In general, it may not be possible to know the exact locations and/or levels of the pressure gradients except for regions of large height discontinuity on the slider surface (Wu *et al.*, 1999, Wu *et al.*, 2000). In order to bring some flexibility to creating the finite element mesh the vertex label based adaptive meshing strategy for quadrilateral elements introduced by Cheng *et al.* (Cheng *et al.*, 1989) is adopted in this work.

The adaptive meshing algorithm, described next, uses the pressure gradient as the metric for making subdivision decisions. A pressure gradient metric is calculated

for each element and then distributed to the each node (called vertex hereafter) of the element. In the vertex label assignment scheme of Cheng et al. (Cheng *et al.*, 1989), subdivision decisions are based on the labels assigned on the vertices of the mesh rather than the subdivision levels assigned to elements. This method ensures *conformity* of the subdivided mesh, where a conforming mesh is defined as a mesh where any two elements either share two pints and one edge, or share one point, or have no edges or points in common. This method prevents creation of dangling nodes that are not attached to another node, and ensures creation of reasonably shaped elements.

### 3.1. Element Level Subdivision Label Assignment

Two factors are considered in making a decision about the subdivision level of a given element. The first is the pressure gradient of the element, and the second is whether the element is located over a step of the slider (Holani, 2002).

Let  $P$  be the regular quadrilateral mesh, and  $V$  and  $F$  be the sets of vertices and elements of  $P$ , respectively. Consider an element  $f \in F$ : the element level subdivision label assignment,  $S$  is indicated by  $S(f)$ . The function  $S$  can be zero or any integer number, (i.e.,  $S: F \rightarrow N \cup \{0\}$  where  $N$  is the set of all positive integers.)

#### 3.1.1. Pressure Gradient Based Subdivision Level, $S_I(f)$

The element subdivision assignment  $S_I$  is an integer value based on the pressure gradient of a given element and the maximum value among all the elements. For *each* element,  $f$ , two element subdivision levels indicated by  $S_{I_x}$  and  $S_{I_y}$  are calculated in the  $x$ - and  $y$ -directions as follows:

$$\text{if } R_{low} \leq \left\{ \frac{dp}{dx} \right\}_{max}^{elem} / \left\{ \frac{dp}{dx} \right\}_{max}^{mesh} \leq R_{high} \text{ then } S_{I_x}(f) = I$$

$$\text{if } R_{low} \leq \left\{ \frac{dp}{dy} \right\}_{max}^{elem} / \left\{ \frac{dp}{dy} \right\}_{max}^{mesh} \leq R_{high} \text{ then } S_{I_y}(f) = I$$

where  $R_{low}$  and  $R_{high}$  are the lower and upper limits of the pressures gradient ratios and  $I \in (N \cup \{0\})$  is an integer value indicating the level of subdivisions. As the pressure gradient ratio approaches 1 the value of  $I$  should be increased to ensure finer refinement. In the implementation, the pressure gradient of each element is checked and an appropriate class number  $C_i$  is assigned for each element. The refinement classes  $C_i$  used in this work are given in Table 1. The refinement level assignments are typically higher for higher classes. For example, a choice could be  $C_1 = C_2 = C_3 = 0$ ,  $C_4 = 1$  and  $C_5 = 2$ . For a given element the maximum of the two refinement levels is used:

$R_{low}$	$R_{high}$	Refinement Class, $C_i$
$1 \times 10^{-4}$	$5 \times 10^{-4}$	1
$5 \times 10^{-4}$	$5 \times 10^{-3}$	2
$5 \times 10^{-3}$	$2.5 \times 10^{-1}$	3
$2.5 \times 10^{-1}$	$8.5 \times 10^{-1}$	4
$8.5 \times 10^{-1}$	1	5

**Table 1.** Limits of the element level, pressure gradient based, adaptation criterion used in Section 3.1.1.

$$S_1(f) = \max(S_{1x}, S_{1y}) \quad (15)$$

### 3.1.2. Step Height Based Subdivision Level, $S_2(f)$

It is extremely important to refine the mesh locally along all of the edges where there is an abrupt change in the height, as this condition causes very large changes in pressure in the vicinity of such edges. It is also important that these refinements be made at the maximum level among the ones mentioned in Section 3.1.1, so that they do not cause any convergence problems. Then the step height based subdivision assignment around the outer periphery of a geometric step is carried out by using the  $S_2$  function:

$$S_2(f) = \max(S_1(f)) \quad (16)$$

### 3.1.3. Effective Adaptation Criterion, $S(f)$

The effective adaptation criterion is defined as follows:

$$S(f) = \max(S_1(f), S_2(f)). \quad (17)$$

It may look odd for a moment, to take the maximum among the two again, where  $S_2$  is already the maximum of the two. However, note that this criterion is only used for the elements associated with edges of the geometry. For all other elements the  $S_2(f) = 0$  (Holani, 2002).

## 3.2. Vertex Label Assignment

Once the element label assignment is made for all elements, the vertex label assignment can be made for all vertices  $v$  ( $v \in V$ ) of the mesh. The vertex label assignment is indicated by the function  $L(v)$ . The vertex label assignment is done in

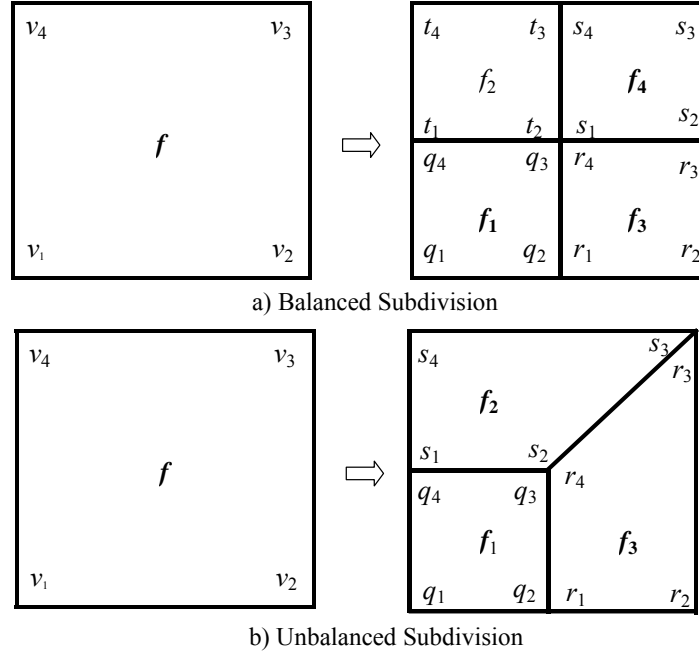


**Figure 2.** a) Balanced and b) unbalanced subdivision of an element.

such a way that for each vertex  $v$ , the vertex label  $L(v)$ , is the maximum of the element labels surrounding that vertex (Cheng *et al.*, 1989). Thus each vertex is assigned either a zero or a positive integer label, (i.e.  $L: V \rightarrow N \cup \{0\}$ .) A vertex label assignment,  $L$ , of  $P$  with respect to  $S$  is a function defined as:

$$L(v) = \max(S(f) \mid f \in F \text{ and } v \text{ is the vertex of } f).$$

In addition to this, to ensure *conformity* requirements of the mesh an *admissible label assignment*  $G(v)$  is defined (Cheng *et al.*, 1989). This assignment, described in Section 3.4, prevents creation of dangling nodes and ensures geometrically well shaped elements.

### 3.3. Element Subdivision

After each vertex is assigned a label the mesh subdivision takes place based on two subdivisions procedures: the balanced subdivision and the unbalanced subdivision (Cheng *et al.*, 1989).

#### 3.3.1. Balanced Subdivision

Consider a four-noded quadrilateral element  $f$ , with vertices  $v_1, v_2, v_3$  and  $v_4$ , indicated by  $f = v_1 v_2 v_3 v_4$ . The *balanced subdivision* is performed on a four-noded

quadrilateral,  $f = v_1 v_2 v_3 v_4$ , having at least two non-zero labels assigned to its vertices. (Exceptions to this are discussed in Section 3.4). At first this procedure generates four sub-quadrilateral elements  $f_1 = q_1 q_2 q_3 q_4$ ,  $f_2 = r_1 r_2 r_3 r_4$ ,  $f_3 = s_1 s_2 s_3 s_4$ ,  $f_4 = t_1 t_2 t_3 t_4$  and assigns a label to each of its vertices as shown in Fig. 2a. The new vertex assignments are defined as follows (Cheng *et al.*, 1989):

$$\begin{aligned} q_1 &= v_1, r_2 = v_2, s_3 = v_3, t_4 = v_4 \\ q_2 &= r_1 = (v_1 + v_2)/2, \quad s_2 = r_3 = (v_2 + v_3)/2 \\ t_3 &= s_4 = (v_3 + v_4)/2, \quad t_1 = q_4 = (v_1 + v_4)/2 \\ q_3 &= r_4 = s_1 = t_2 = (v_1 + v_2 + v_3 + v_4)/4 \end{aligned}$$

The label assignments for the new vertices are as follows:

$$\begin{aligned} L(q_1) &= \max(0, L(v_1) - 1); L(r_2) = \max(0, L(v_2) - 1) \\ L(s_3) &= \max(0, L(v_3) - 1); L(t_4) = \max(0, L(v_4) - 1) \\ L(q_2) &= L(r_1) = \min(L(q_1), L(r_2)); L(r_3) = L(s_2) = \min(L(r_2), L(s_3)) \\ L(s_4) &= L(t_3) = \min(L(s_3), L(t_4)); L(t_1) = L(q_4) = \min(L(t_4), L(q_1)) \end{aligned}$$

$$\begin{aligned} \text{if } (L(q_2) = L(r_3) = L(s_4) = L(t_1) = 0) \\ L(q_3) &= L(r_4) = L(s_1) = L(t_2) = 0 \end{aligned}$$

**else**

$$L(q_3) = L(r_4) = L(s_1) = L(t_2) = \max(L(v) | v \in \{q_2, r_3, s_4, t_1\}, L(v) > 0).$$

### 3.3.2. Unbalanced Subdivision

The *unbalanced subdivision* is performed on a four-noded quadrilateral,  $f = v_1 v_2 v_3 v_4$ , having exactly one non-zero label assigned to any one of its vertices (Cheng *et al.*, 1989). This procedure generates three sub quadrilaterals  $f_1 = q_1 q_2 q_3 q_4$ ,  $f_2 = r_1 r_2 r_3 r_4$ ,  $f_3 = s_1 s_2 s_3 s_4$ , and assigns a label to each of its vertices. For instance if  $v_1$  is the vertex with the non-zero label then the vertices and the labels are defined as shown in Fig. 2b. The new vertices are defined as follows (Cheng *et al.*, 1989):

$$\begin{aligned} q_1 &= v_1, r_2 = v_2, r_3 = s_3 = v_3, s_4 = v_4 \\ q_2 &= r_1 = (v_1 + v_2)/2, \quad s_1 = q_4 = (v_1 + v_4)/2 \\ s_2 &= q_3 = r_4 = (v_1 + v_2 + v_3 + v_4)/4 \end{aligned}$$

The label assignments for the new vertices are as follows (Cheng *et al.*, 1989):

$$\begin{aligned} L(q_1) &= L(v_1) - 1 \\ L(q_i) &= L(r_i) = L(s_i) = 0, \text{ for } i = 2, 3, 4 \end{aligned}$$

Refining of elements requires a conforming refinement of the neighboring elements if the subdivision levels are not equal. This is done by creating appropriate transition elements. The choice of these transition elements could yield bad results, if elements with very acute angles are constructed. The reason for this is that in the second refinement step elements with sharp angles are split up which leads to the

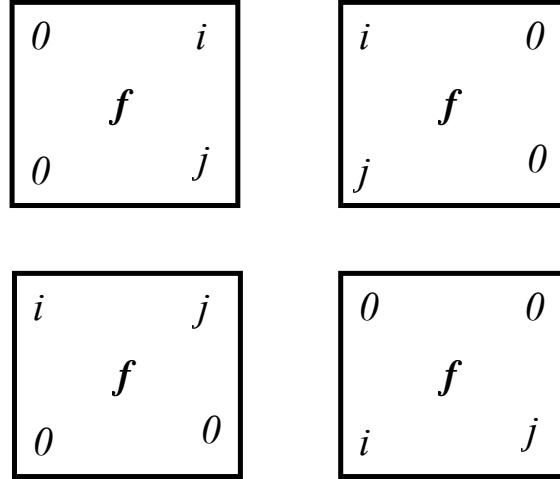


**Figure 3.** Inadmissible vertex label assignments

creation of elements with even more acute angles. Cheng et al. showed a way to overcome this difficulty for structured meshes (Cheng *et al.*, 1989), discussed next.

### 3.4 Admissible Label Function

A label assignment is *non-admissible* if it contains one of the four cases shown in Fig 3 (Cheng *et al.*, 1989). It can easily be shown that such an assignment in a mesh leads to non-conforming elements, which manifest themselves most commonly with dangling nodes, i.e. nodes that do not belong to the vertex set of some of the adjacent elements. Cheng et al. have devised an admissible function construction, which removes such cases without violating the conformity requirement (Cheng *et al.*, 1989). Their algorithm is based on a regular quadrilateral network whose vertices form an  $m \times n$  rectangular grid,  $V = \{v_{i,j} | 1 \leq i \leq m, 1 \leq j \leq n\}$ . In case the mesh is not a regular quadrilateral mesh, they suggest using fictitious nodes to render it quadrilateral, and to remove the fictitious nodes once the algorithm is complete. An element  $f_{i,j}$  is defined by four vertices  $v_{i,j}$ ,  $v_{i+1,j}$ ,  $v_{i,j+1}$ ,  $v_{i+1,j+1}$ .

The label assignment  $L$  on  $V$  can be rendered an admissible label assignment  $G$  by applying the algorithm specified by Cheng et al. (Cheng *et al.*, 1989). First, two special functions  $L_o$  and  $L_e$  are defined for use in the algorithm as follows (Cheng *et al.*, 1989):

$$L_o(v_{i,j}) = \begin{cases} 1 & \text{if } i+j \text{ is odd} \\ \frac{1}{2} & \\ 0 & \text{if } i+j \text{ is even} \end{cases}$$

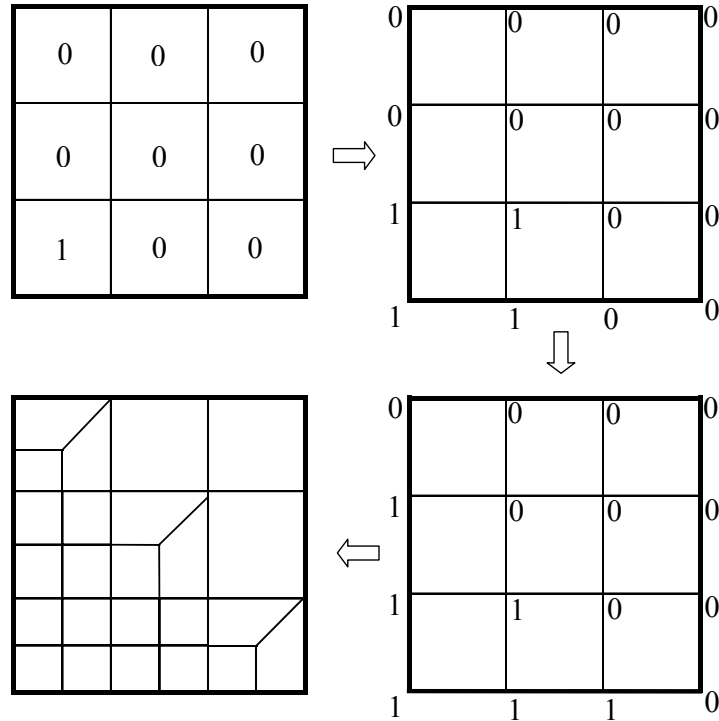


**Figure 4.** Admissible label assignment

$$L_e(v_{i,j}) = \begin{cases} \frac{1}{2} & \text{if } i+j \text{ is even} \\ 0 & \text{if } i+j \text{ is odd} \end{cases}$$

The algorithm to construct the admissible label assignment function  $G$  is as follows (Cheng *et al.*, 1989):

1. Construct  $G_e$ 
  - for** each  $v_{i,j}$
  - $G_e(v_{i,j}) = \max(L, L_e(v_{i,j}))$
  - for** each  $v_{i,j}$  such that  $G_e(v_{i,j}) = \frac{1}{2}$
  - if**  $G_e(v_{i,j}) > \frac{1}{2}$  for at least one adjacent vertex of  $v_{i,j}$
  - then**  $G_e(v_{i,j}) = 1$
  - else**  $G_e(v_{i,j}) = 0$ .
2. Construct  $G_o$ 
  - for** each  $v_{i,j}$

```

do  $k = 1, 2$ 

  if  $k = 1$  set uniform mesh

  if  $k = 2$  then
    calculate mesh adaptation criteria
    perform mesh adaptation
    minimize bandwidth
    use  $p$  and  $\Psi$  from  $k = 1$  as initial guess
  endif

  repeat until  $\varepsilon_s < 10^{-2}$ 

    repeat until  $\varepsilon_p < 10^{-2}$ 
      Solve  $\mathbf{K}_p^{(m)} \mathbf{dP}^{(m)} = \mathbf{R}_p^{(m)}$ 
       $\mathbf{P}^{(m+1)} = \mathbf{P}^{(m)} + \mathbf{dP}^{(m)}$ 
    end repeat

    Solve  $\mathbf{K}_\Psi^{(n)} \Psi^{(n)} = \mathbf{R}^{(n)}$ 
  end repeat
end do

```

**Figure 5.** Flowchart for the entire code developed during the course of this work.

$$G_o(v_{i,j}) = \max(L, L_o(v_{i,j}))$$

**for** each  $v_{i,j}$  such that  $G_e(v_{i,j}) = \frac{1}{2}$

**if**  $G_o(v_{i,j}) > \frac{1}{2}$  for at least one adjacent vertex of  $v_{i,j}$

**then**  $G_o(v_{i,j}) = 1$

**else**  $G_o(v_{i,j}) = 0$ .

3. Construct  $G$

**if**  $|V_0^{G_o}| > |V_0^{G_e}|$

**then** return  $G = G_e$

**else** return  $G = G_o$ ,

where  $V_0^{G_o}$  is the set of vertices  $v_{i,j}$  such that  $G_{e,o}(v_{i,j}) = 0$ . Looking at the example, shown in Fig. 4, after the vertex label assignment is done, the algorithm assigns labels to all the four nodes of only that element. If admissible label assignment is performed on this set of labels, it yields another set of labels with more positive

labels, as shown in the Fig. 4, which on subdivision prevents the creation of the dangling nodes.

### 3.5. Mesh Clean Up and Bandwidth Reduction

Once the subdivision on the mesh is performed with the admissible label assignment, the problem of the dangling nodes is taken care of. However, clean up is still required on the resultant mesh to maintain the conformity requirement. The nodes with more than one node number assignment, as a result of subdivision, need to be handled. In this work, when such a node is encountered the program removes the higher of the node numbers, decreases the node numbers correspondingly, and finally, adjusts the element connectivity matrix.

The addition of new nodes changes the node numbering scheme and consequently the bandwidth of the global stiffness matrix. Bandwidth reduction is an important issue as Eqns (11) and (14) are solved by a direct solver. In this work, the algorithm proposed by Collins (Collins, 1973) for the bandwidth reduction is implemented.

### 3.6. Adaptive Meshing Strategy

In this work the mesh subdivision is performed in two steps (Holani, 2002). First the domain is discretized into a regular rectangular mesh and the coupled solution of Eqns (2) and (3) is found. Second, the mesh subdivision assignments, as described in Sections 3.1 - 3.4 are performed, and the coupled solution of Eqns. (2) and (3) is found for the second time. The algorithm of the method is presented in Fig 5.

In either one of the solutions the steady state position for a slider is obtained by solving Eqns (4) and (12) iteratively. After choosing an initial solution, the solution is repeated in an iterative manner until convergence is achieved. The criterion for convergence for both the pressure solution and the slider position, are as follows:

$$\varepsilon_p = \frac{1}{n_d \varepsilon_p^{(1)}} \left[ \sum_{i=1}^{n_d} \left\{ \frac{p_i^{(n+1)} - p_i^{(n)}}{p_i^{(n)}} \right\}^2 \right]^{\frac{1}{2}} \quad (18)$$

$$\varepsilon_s = \frac{1}{\varepsilon_s^{(1)}} \left[ \left\{ \frac{h^{(n+1)} - h^{(n)}}{h^{(n)}} \right\}^2 + \left\{ \frac{\alpha^{n+1} - \alpha^{(n)}}{\alpha^{(n)}} \right\}^2 + \left\{ \frac{\beta^{(n+1)} - \beta^{(n)}}{\beta^{(n)}} \right\}^2 \right]^{\frac{1}{2}} \quad (19)$$

where  $\varepsilon_p$  is the error in the pressure distribution,  $\varepsilon_s$  is the error in the slider position, and  $\varepsilon_p^{(1)}$  and  $\varepsilon_s^{(1)}$  are the error values in the first iteration. Convergence is achieved when the following equation is satisfied simultaneously,

$$\varepsilon_p, \varepsilon_s \leq 0.01 \quad (20)$$

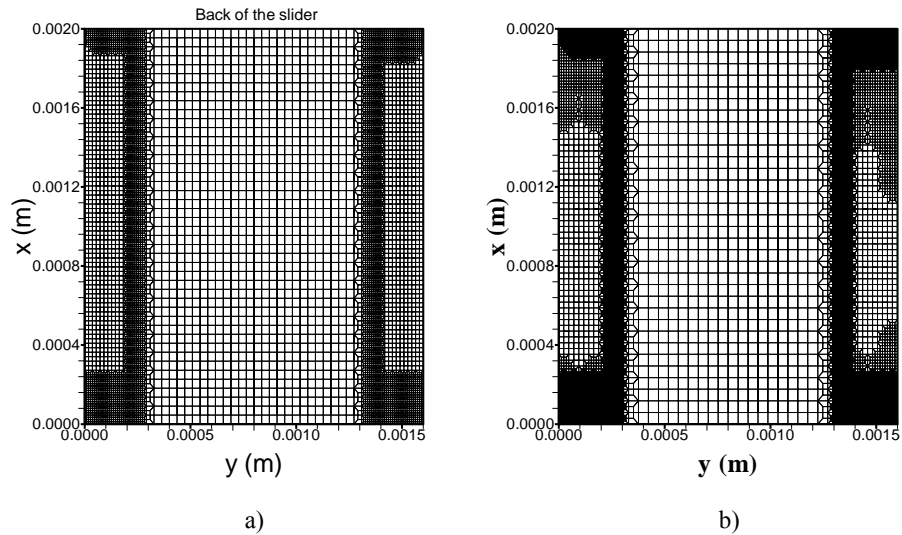


**Figure 6.** Mesh layout for the taper slider a) with two subdivision levels (initial mesh:  $45 \times 45$  nodes; adapted mesh: 8345 nodes, 8153 elements), b) with three subdivision levels (initial mesh:  $35 \times 35$  nodes; adapted mesh: 16790 nodes, 16534 elements).

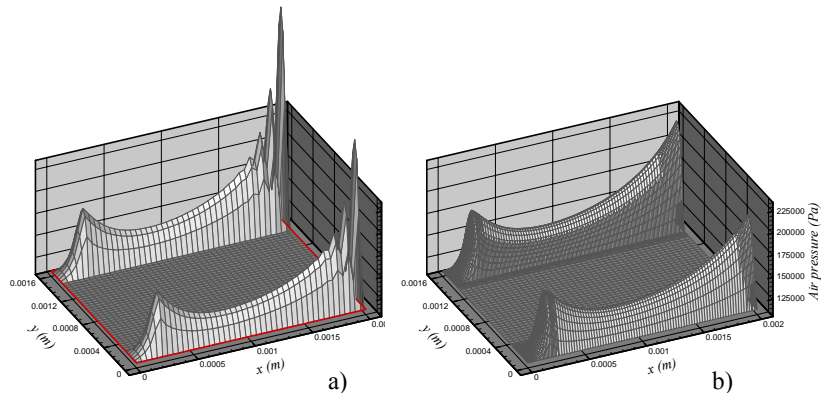


**Figure 7.** Comparison of the air pressure distributions under the 50% slider with a) Uniform  $45 \times 45$  mesh, and b) with the mesh given in Figure 6a.

#### 4. Results and Discussion

The numerical design simulator for the head disk interface has been applied to two different slider geometries, one of them is a 50% taper-flat, two-rail slider and the other is a negative pressure air bearing slider.

#### 4.1. 50% Taper-Flat, Two-Rail Slider

The parameters of the taper-flat slider modeled are tabulated in Table 2. The initial mesh consists of regular rectangular four noded elements. After adaptation, various finite element meshes with different adaptation levels are shown in Fig. 6. Fig. 6a shows a mesh initially with 2025 (45×45) nodes, with a maximum adaptation level of two, resulting in 8345 nodes and 8153 four noded elements. The refinement class assignments for this case were  $C_1 = C_2 = 0$ ,  $C_3 = C_4 = 1$  and  $C_5 = 2$ . Fig. 6b shows a mesh initially with 1225 (35×35) nodes, with a maximum adaptation level of three, resulting in 16790 nodes and 16534 four noded elements. The refinement class assignments for this case were  $C_1 = C_2 = 0$ ,  $C_3 = 1$ ,  $C_4 = 2$  and  $C_5 = 3$ . Observe that the mesh density is high at the trailing edge, and at the intersection of the taper with the flat surface. Also the mesh is refined at the steps where a large change in slider height is detected.

A typical 2D pressure profile for this air bearing is shown in Fig. 7. The solution shows two pressure peaks on each rail, one at the trailing edge of the rail and the other at the rail-taper intersection. The pressure profile given in Fig. 7a was calculated with an initial mesh of 2025 (45×45) nodes. The mesh size is insufficient to resolve the pressure gradients at the trailing edge region.

Parameter	
Slider type	50% taper flat, two-rail
Length	2.0 mm
Width	1.6 mm
Rail width	0.25 mm
Taper angle	8.7 mrad
Taper length	0.2 mm
Preload	35 mN
Velocity	10 m/s
Pivot Point, $x$ -coordinate	0.889 mm
Pivot Point, $y$ -coordinate	0.7746 mm
Atmospheric Pressure	101300 Pa
Viscosity	$18.34 \times 10^{-6}$ N./m <sup>2</sup>
Molecular mean free path (Air)	$63.5 \times 10^{-9}$ m
Slip flow correction	Second order
Vertical suspension stiffness	18 N/m
Rotational flexure stiffness (Pitch)	1.0e-6 N/deg
Rotational flexure stiffness (Roll)	1.0e-6 N/deg

**Table 2.** Model parameters for the 50% taper flat, two-rail slider bearing.

The refined mesh given in Fig. 6a, which has 8345 nodes, was used to obtain the results given in Fig. 7b. Observe that the pressure distribution is very smooth with the adapted mesh when compared with the one with the initial mesh. This refinement is done automatically in the software.

#### 4.2 Negative Pressure Air Bearing Slider

A schematic of a negative pressure slider is shown in Fig. 8. Typical overall dimensions of the slider are  $1.25 \times 1$  mm. Areas A, C and E, marked with a checkerboard pattern are at the same height level, and they are  $4 \mu\text{m}$  above the unmarked white area. The areas B and D, marked with cross-hatched lines, are 200 nm tall protrusions with respect to areas A, C and E. The pivot point is at the geometric center of the slider, other parameters, such as viscosity, velocity, stiffness are same those used for taper flat slider, given in Table 2. The pre-load on the slider is 35 mN and the inertia effects are neglected.

The initial mesh consists of regular rectangular four noded elements. Two finite element meshes with different adaptation levels are shown in Fig 9. Part-a of this figure shows a mesh initially with 6516 ( $81 \times 81$ ) nodes, with a maximum adaptation level of one, resulting in 13505 nodes and 13327 quadrilateral elements. The refinement class assignments for this case were  $C_1 = C_2 = C_3 = 0$ ,  $C_4 = 1$  and  $C_5 = 1$ . Fig. 9b shows a mesh initially with 7569 ( $87 \times 87$ ) nodes, with a maximum adaptation level of two, resulting in 15519 nodes and 15338 four noded elements. The refinement class assignments for this case were  $C_1 = C_2 = C_3 = 0 = C_4 = 1$  and  $C_5 = 2$ . Observe that the mesh density is high at the trailing edge. Also the mesh is refined at the steps where a large change in slider height exists.

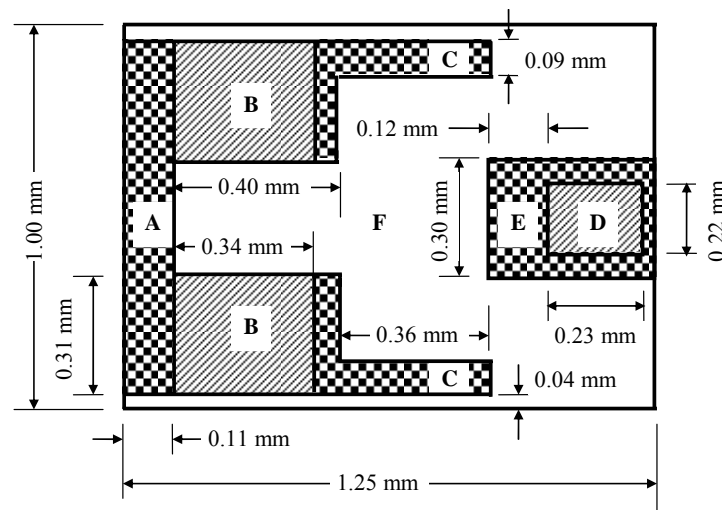


**Figure 8.** Geometry of the negative pressure air bearing slider

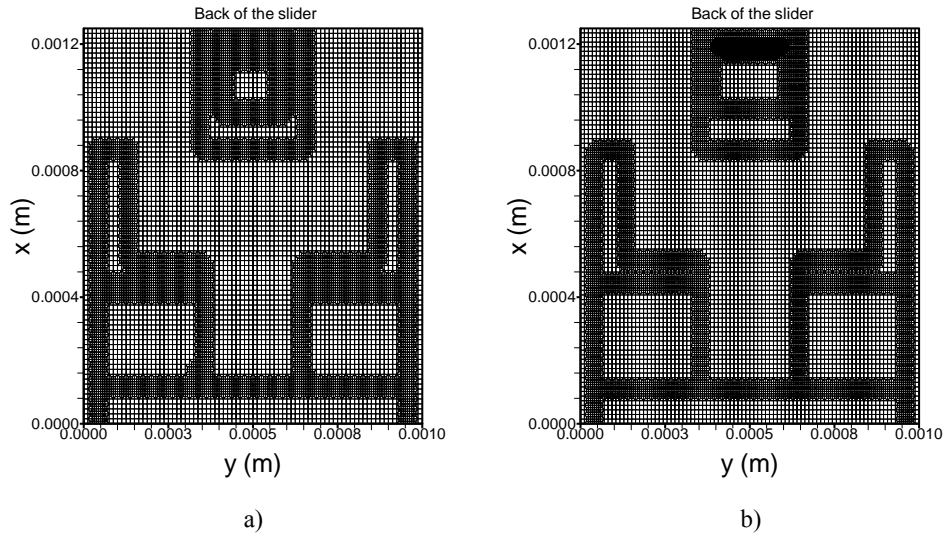


**Figure 9.** Mesh layout for the negative bearing slider a) with one subdivision levels (initial mesh:  $81 \times 81$  nodes; adapted mesh: 13505 nodes, 13327 elements), b) with two subdivision levels (initial mesh:  $87 \times 87$  nodes; adapted mesh: 15519 nodes, 15338 elements).

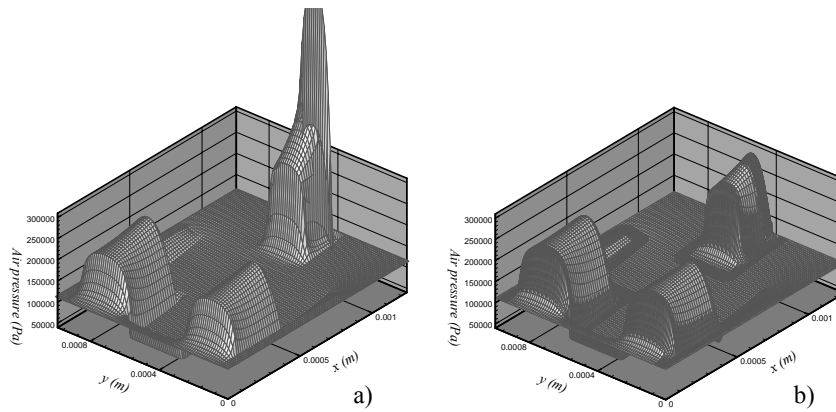


**Figure 10.** Comparison of the air pressure distributions under the negative bearing slider with a) Uniform  $87 \times 87$  mesh, and b) with the mesh given in Figure 9b.

Pressure distribution under the negative air bearing slider is shown in Fig. 10. In general, three pressure peaks occur, one at the trailing edge of the slider and two at the rear ends of the front pads. Fig. 10 shows the 3D pressure distribution for the air bearing with an initial mesh of 6561 (81×81) nodes in part-a, and with an adapted mesh having 15519 nodes in part-b. Observe that the pressure distribution is very smooth with the adaptively refined mesh, when compared with the one with the initial mesh-

## 6. Summary, Conclusions and Future Work

This paper provides a numerical design tool to analyze the head-disk interface for magnetic head sliders used in hard disk drives. The finite element method has been used discretize modified Reynolds equation. The hydrodynamic stiffness approach has been implemented to improve the solution of the coupled system of air lubrication and slider equilibrium equations. An adaptive mesh algorithm is implemented to capture the fine aspects of the slider geometry, and regions of high pressure gradients. A bandwidth reduction algorithm has been applied for efficient memory management and minimizing computational time.

Two sliders have been analyzed, namely the 50% taper flat slider, and a negative air bearing slider. It was shown that using the adaptive mesh gives more flexibility and control over the placement of nodes, and also enables the user to obtain smooth pressure contours with considerably less effort. Improvements to this work in the future should include a) placement of nodes exactly on the recess boundaries, b) implementation of iterative solution scheme, c) implementation of contact pressure between the disk and the slider.

## References

- Bhushan, B., *Tribology and Mechanics of Magnetic Storage Devices*, McGraw-Hill, Second Edition, 1996.
- Burgdofer, A., "The Influence of Molecular Mean Free Path on the Performance of Hydrodynamic Gas Lubricated Bearings", *Transactions ASME, Journal of Basic Engineering*, Vol. 81, no. 1, 1959, pp. 94-100.
- Castelli, V., and Pirvics, J., "Review of Numerical Methods in Gas Bearing Film Analysis", *ASME Journal of Lubrication Technology*, Oct 1968, pp. 777-792.
- Cheng, F., Jaromczyk, J. W., Lin, J.-R., Chang, S.-S., Lu, J.-Y., "A Parallel Mesh Generation Algorithm Based on the Vertex Label Assignment Scheme", *International Journal of Numerical Methods in Engineering*, Vol. 28, 1989, pp. 1429-1448.
- Choi, D.H., Yoon, S.J., "Static analysis of flying characteristics of the head slider by using an optimization technique," *Journal of Tribology, Transactions of the ASME*, Vol. 116, No. 1, pp. 90-94, 1994.
- Collins, R. J., "Bandwidth Reduction by Automatic Renumbering", *International Journal of Numerical Methods in Engineering*, Vol. 6, 1973, pp. 345-356

- Crone, R.M, Jhon, M.S., Karis, T.E., and Bhushan. B., "The behavior of a magnetic slider over a rigid disk surface: A comparison of several approximations of the modified Reynolds equations," *Adv. Info. Storage Syst.*, Vil. 4, pp.105-121, 1992.
- Fukui, S. and Kaneko, R., "Analysis of Ultra-Thin Gas Film Lubrication Based on Linearized Boltzmann Equation: First report-Derivation of a Generalized Lubrication Equation Including Thermal Creep Flow," *Trans. ASME Journal of Tribology*, Vol. 110, pp. 253-261, 1988.
- Fukui, S. and Kaneko, R., "A database for interpolation of Poiseuille flow rates for high Knudsen number lubrication problems," *Trans. ASME Journal of Tribology*, Vol. 112, pp. 78-83, 1990.
- Garcia-Suarez, C., Bogy, D.B., and Talke, F.E., "Use of an Upwind Finite Element scheme for Air Bearing Calculations", *Tribology and Mechancis of Magnetic Storage Systems*, ASLE, Vol. 1, 1984, pp. 90-96.
- Hendricks, F., "A Design Tool for Steady State Gas Bearings using Finite Elements, the APL language and Delaunay Triangulation", *Tribology and Mechancis of Magnetic Storage Systems*, ASLE, Vol. 5, 1988, pp. 124-129.
- Holani, P. "Finite Element Analysis of the Head Disk Interface in a Hard Disk Drive using an Adaptive Mesh," M.S. Thesis, Northeastern University, August 2002.
- Hsia, Y. T., and Domoto, G. A., "An Experimental Investigation of Molecular Rarefaction Effects in Gas Lubricated Bearings at Ultra-Low Clearances", *Transactions ASME*, Vol. 105, 1983, pp. 120-130.
- Kubo, M., Ohtsubo, Y., Kawashima, N., Marumo, H., "Finite element solution for the rarefied gas lubrication problem," *Journal of Tribology*, *Transactions of the ASME*, Vol. 110, No. 2, pp. 335-341, 1988.
- Mee, C.D. and Daniel, E.D., *Magnetic Recording Technology*, McGraw-Hill, Second Edition, 1996.
- Miu, D.K., and Bogy, D.B., "Dynamics of Gas-Lubricated Slider Bearing in Magnetic Recording Disk Files – Part II: Numerical simulation," *Journal of Tribology*, *Transactions of the ASME*, Vol. 108, pp. 589-593.
- Ono, K., "Dynamic Characteristics of the air-lubricated slider bearing for non-contact magnetic recording," *ASME Journal of Lubrication Technology*, Vol. 97, No. 2, pp. 250-260, 1972.
- Peng, J.-P., Hardie, C.E., "A finite element scheme for determining the shaped rail slider flying characteristics with experimental confirmation," *Journal of Tribology*, *Transactions of the ASME*, Vol. 117, pp. 358-364, 1995.
- Smith, P. W., Wahl, M. H., and Talke, F. E., "Accelerated natural convergence for pivoted slider bearings" *Tribology Transactions*, Vol. 38, No. 3, Jul. 1995, pp. 595-600

- Tang, T., "Dynamics of air-lubricated slider bearings for non-contact magnetic recording," ASME Journal of Lubrication Technology, Vol. 93, No. 2, pp. 272-278, 1972.
- Wahl, M. H., "Numerical and Experimental Investigation of the Head/Disk Interface", Ph.D. Dissertation, University of California, San Diego, 1994.
- White, J. W., "Flying Characteristics of the 3370-Type Slider on a 5.25-inch Disk – Part-1: Static Analysis", Tribology and Mechanics of Magnetic Storage Systems, Vol. 1, 1984, pp. 72-76.
- White, J. W., and Nigam, A., "A Factored Implicit Scheme for the Numerical Solution of the Reynolds equation at Very Low Spacing", ASME Journal of Lubrication Technology, Vol. 102, 1980, pp. 80-85.
- Wu, L., Bogy, D. B., "Unstructured Adaptive Triangular Mesh Generation Techniques and Finite Volume Schemes for the Air Bearing Problem in Hard Disk Drives", ASME Journal of Tribology, Vol. 122, Oct. 2000, pp. 761-770.
- Wu, L., Bogy, D. B., "Unstructured Triangular Mesh Generation Techniques and a Finite Volume Scheme for Slider Air Bearing Simulation with Complex Shaped Rails", IEEE Transactions on Magnetics, Vol. 35, No.5, pp 2421-2423, 1999.
- Yamaura, H., and Ono, K., "Inverse analysis of flying height slider bearings for magnetic disk recording," Proceedings of the Japan Int. Trib. Conf., Nagoya, 1990, pp. 1917-1922.
- Zienkiewicz, O. C., and Taylor, R. L., "The Finite Element Method", Vol. 1, Butterworth Heinemann, Fifth Edition, 2000.

### Appendix 1

Using bilinear shape functions, four point Gauss quadrature, the components of the element stiffness matrix for eqn. (10) become,

$$\begin{aligned}
 \mathbf{K}_{\psi_{i,j}}^{(e)} &= \\
 &= \Pi_{2 \times 2} \left\{ \begin{aligned} &\left( \left( h^{(n)} \right)^3 + 6 p_a \lambda_a \frac{\left( h^{(n)} \right)^2}{p^{(n)}} - 6 (p_a \lambda_a)^2 \frac{h^{(n)}}{\left( p^{(n)} \right)^2} \right) \left( \frac{\partial p^{(n)}}{\partial x} \frac{\partial N_i}{\partial x} + \frac{\partial p^{(n)}}{\partial y} \frac{\partial N_i}{\partial y} \right) N_j + \\ &\left( \left( h^{(n)} \right)^3 p^{(n)} + 6 p_a \lambda_a \frac{\left( h^{(n)} \right)^2}{p^{(n)}} + 6 (p_a \lambda_a)^2 \frac{h^{(n)}}{p^{(n)}} \right) \left( \frac{\partial N_j}{\partial x} \frac{\partial N_i}{\partial x} + \frac{\partial N_j}{\partial y} \frac{\partial N_i}{\partial y} \right) + \\ &6 \mu N_i \left( h^{(n)} \left( V_x \frac{\partial N_j}{\partial x} + V_y \frac{\partial N_j}{\partial y} \right) + N_j \left( V_x \frac{\partial h^{(n)}}{\partial x} + V_y \frac{\partial h^{(n)}}{\partial y} \right) \right) \end{aligned} \right\} \det J,
 \end{aligned} \tag{A.1}$$

and the elements of the right hand side vector for eqn. (10) become,

$$\begin{aligned}
 \mathbf{r}_{\psi_i}^{(e)} &= \\
 &= -\Pi_{2 \times 2} \left\{ \begin{aligned} &\left( 3 p^{(n)} \left( h^{(n)} \right)^2 + 6 \frac{\left( p_a \lambda_a \right)^2}{p^{(n)}} + 12 \left( p_a \lambda_a \right) h^{(n)} \right) \left( \frac{\partial p^{(n)}}{\partial x} \frac{\partial N_i}{\partial x} + \frac{\partial p^{(n)}}{\partial y} \frac{\partial N_i}{\partial y} \right) + \\ &6 \mu N_i \left( V_x \frac{\partial p^{(n)}}{\partial x} + V_y \frac{\partial p^{(n)}}{\partial y} \right) \end{aligned} \right\} \det J.
 \end{aligned} \tag{A.2}$$

where  $i, j = 1, 2, 3, 4$ . In these equations  $N_i$  are the bilinear shape functions and  $J$  is the Jacobian. The operator  $\Pi_{2 \times 2}$  represents four point Gauss quadrature.

## Appendix 2

Using bilinear shape functions, four point Gauss quadrature, the components of the element stiffness matrix for eqn. (13) become,

$$\begin{aligned} \mathbf{k}_{p_i, j}^{(e)} &= \\ &= \Pi_{2 \times 2} \left\{ \begin{aligned} &\left( h^{(m)3} - 6(p_a \lambda_a)^2 \frac{h^{(m)}}{p^{(m)2}} \right) \left( \frac{\partial p^{(m)}}{\partial x} \frac{\partial N_i}{\partial x} + \frac{\partial p^{(m)}}{\partial y} \frac{\partial N_i}{\partial y} \right) N_j + \\ &\left( h^{(m)3} p^{(m)} + 6p_a \lambda_a h^{(m)2} + 6(p_a \lambda_a)^2 \frac{h^{(m)}}{p^{(m)}} \right) \left( \frac{\partial N_j}{\partial x} \frac{\partial N_i}{\partial x} + \frac{\partial N_j}{\partial y} \frac{\partial N_i}{\partial y} \right) + \\ &6\mu N_i \left( h^{(m)} \left( V_x \frac{\partial N_j}{\partial x} + V_y \frac{\partial N_j}{\partial y} \right) + N_j \left( V_x \frac{\partial h^{(m)}}{\partial x} + V_y \frac{\partial h^{(m)}}{\partial y} \right) \right) \end{aligned} \right\} \det J. \end{aligned} \quad (\text{A.3})$$

and the elements of the right hand side vector for eqn. (13) become,

$$\begin{aligned} \mathbf{r}_{p_i}^{(e)} &= \\ &= -\Pi_{2 \times 2} \left\{ \begin{aligned} &\left( p^{(m)} h^{(m)3} + 6p_a \lambda_a h^{(m)2} + 6(p_a \lambda_a)^2 \frac{h^{(m)}}{p^{(m)}} \right) \left( \frac{\partial p^{(m)}}{\partial x} \frac{\partial N_i}{\partial x} + \frac{\partial p^{(m)}}{\partial y} \frac{\partial N_i}{\partial y} \right) + \\ &6\mu N_i \left( p^{(m)} \left( V_x \frac{\partial h^{(m)}}{\partial x} + V_y \frac{\partial h^{(m)}}{\partial y} \right) + h^{(m)} \left( V_x \frac{\partial p^{(m)}}{\partial x} + V_y \frac{\partial p^{(m)}}{\partial y} \right) \right) \end{aligned} \right\} \det J. \end{aligned} \quad (\text{A.4})$$

where  $i, j = 1, 2, 3, 4$ .